EUROfusion

EUROFUSION WPBOP–PR(15)01

J. Linares et al.

Supercritical CO_2 Brayton Power Cycles for DEMO Fusion Reactor Based on Dual Coolant Lithium Lead Blanket

Preprint of Paper to be submitted for publication in Energy

This work has been carried out within the framework of the EUROfusion Consortium and has received funding from the Euratom research and training programme 2014-2018 under grant agreement No 633053. The views and opinions expressed herein do not necessarily reflect those of the European Commission.

Supercritical CO_2 Brayton power cycles for DEMO fusion reactor based on Dual Coolant Lithium Lead blanket

José Ignacio Linares[1], Alexis Cantizano[2], Beatriz Yolanda Moratilla[3], Víctor Martín[4], Lluis Batet[5]

[1]Comillas Pontifical University. Alberto Aguilera, 25 – 28015 Madrid. Spain
linares@comillas.edu

[2]Comillas Pontifical University. Alberto Aguilera, 25 – 28015 Madrid. Spain
alexis.cantizano@comillas.edu

[3]Comillas Pontifical University. Alberto Aguilera, 25 – 28015 Madrid. Spain
ymoratilla@comillas.edu

[4]Comillas Pontifical University. Alberto Aguilera, 25 – 28015 Madrid. Spain
victor.marpal@gmail.com

[5]Catalonia Polytechnical University. Diagonal, 647 – 08028 Barcelona. Spain
lluis.batet@upc.edu

Corresponding author:

José Ignacio Linares
[1]Comillas Pontifical University. Alberto Aguilera, 25 – 28015 Madrid. Spain
linares@comillas.edu
Phone: 0034 91 542 28 00, ext. 2368

Supercritical CO_2 Brayton power cycles for DEMO fusion reactor based on Dual Coolant Lithium Lead blanket

J.I. Linares[1,*], A. Cantizano[1], B.Y. Moratilla[1], Víctor Martín[1], Lluis Batet[2]

[1]Comillas Pontifical University. Alberto Aguilera, 25 – 28015 Madrid. Spain

[2]Catalonia Polytechnic University. Diagonal, 647 – 08028 Barcelona. Spain

[*]Corresponding author (linares@comillas.edu)

ABSTRACT

Fusion energy is one of the most promising solutions to the world's energy supply. This paper presents an exploratory analysis of the suitability of supercritical CO_2 Brayton power cycles as alternative energy conversion systems for a future fusion reactor based on a dual coolant lithium-lead (DCLL) blanket, as prescribed by EUROfusion. The main issue dealt is the optimization of the integration of the different thermal sources with the power cycle (up to four at different power and temperature levels) in order to achieve the highest electricity production. The analysis includes the assessment of the pumping consumption both in the source loops as in the sink one. Other considerations, as control issues and integration of thermal energy storage systems to face the pulsed operation, have been also taken into account. An exergy analysis has been performed in order to understand the behavior of each layout.

Up to ten scenarios have been analyzed, taking into account the heat power released from some thermal sources directly to the sink and assessing different locations for thermal sources heat exchangers. Neglecting the worst four scenarios, it is observed less than 2% of variation among the other six ones. One of the best six scenarios clearly stands out over the others due to the location of the thermal sources in a unique island, being this scenario compatible with the control criteria. In this proposal 34.6% of electric efficiency (before the self-consumptions of the reactor but including pumping consumptions and generator efficiency) is achieved.

KEYWORDS: balance of plant, fusion power, supercritical CO_2 Brayton cycle, DCLL, DEMO

Highlights:

> Supercritical CO_2 Brayton cycles have been proposed for BoP of DCLL fusion reactor.

> Integration of different available thermal sources has been analyzed considering ten scenarios.

> Neglecting the four worst scenarios the electricity production varies less than 2%.

> Control and energy storage integration issues have been considered in the analysis.

> Discarding the vacuum vessel and joining the other sources in an island is proposed.

1. INTRODUCTION

Fusion energy is one of the most promising solutions to the world´s energy problem. Among its most outstanding features are intrinsic safety, management of environmental impact, and long-term availability of primary fuels (deuterium and lithium). In view of that potential, the European Commission requested EFDA (European Fusion Development Agreement) to prepare a technical roadmap to achieve fusion electricity by 2050 [1]. This included two main milestones: ITER (International Tokamak Experimental Reactor) and DEMO (DEMOnstration Power Plant). The main objective of ITER is to demonstrate the technological feasibility of fusion energy by producing net thermal energy and testing the required materials [2]. DEMO will be a bridge between ITER and commercial fusion power plants, demonstrating the feasibility of the integration of all the required systems (reactor and balance of plant) to operate a fusion power plant, including issues of security, wastes management, maintenance, and so on. The main factors affecting the cost of fusion energy are clearly identified [1], being a relevant issue the power conversion cycle, which is strongly conditioned by the chosen model reactor. As a consequence, the EUROfusion consortium (former EFDA) strategy includes a program for Balance of Plant (BoP) modeling, analysis and evaluation [3].

The breeding blanket is the main thermal source for the power conversion cycle in a fusion reactor. Depending on its cooling medium, four types of blankets are distinguished: Water Cooled Lithium Lead (WCLL), Helium Cooled Lithium Lead (HCLL), Dual Cooled Lithium Lead (DCLL), and Self Cooled Lithium Lead (SCLL). The second thermal source in order of importance is the divertor, a device devoted to collect the plasma waste. This thermal source can operate at high (above 500 ºC) or low temperature (below 250 ºC), depending on the coolant medium (helium for high and water for low temperature). Finally, the vacuum vessel cooling can also supply heat to the conversion power cycle, although in the lowest temperature and power range [4].

DCLL blanket is considered as a mid-term option for fusion power plants with medium (500 ºC) and high temperatures (700 ºC) in the long-term. The coolants are an eutectic of lithium-lead (LL) and helium (He), avoiding the use of water which exhibits complex problems due to its interaction with tritium. Although helium is used as coolant, it only removes part of the power released by the blanket (around 40%), so the pumping power is lower than in a HCLL blanket. The high temperature range of the long-term blanket entails the use of Brayton power cycles which do not use water as working fluid, simplifying the tritium removal again. These high temperature blanket Brayton cycles using helium as working fluid were analyzed in [5], concluding that the expected temperatures are not high enough to achieve high efficiencies. This type of power cycles require temperatures in the range of 850-900 ºC to achieve good efficiencies, as found for Very High Temperature Reactors (VHTR) in fission Generation IV designs [6]. In the case of mid-term blanket design (temperatures lower than 500 ºC) the use of supercritical CO_2 as working fluid in the Brayton cycle (S-CO_2) is more promising, as it has been

explored in Sodium Fast Reactors (SFR) in Generation IV designs [7]. In these types of power plants the S-CO_2 cycle has revealed as an advantageous alternative to more classical Rankine cycles, both supercritical and subcritical configurations [8]. Medrano et al. [9] have analyzed the feasibility of the S-CO_2 cycle as an alternative to steam Rankine cycles in fusion reactors based on HCLL blankets. Ishiyama et al. [10] studied the use of S-CO_2, steam Rankine and helium Brayton cycles for fusion reactors based on both HCLL and WCLL blankets. In [11] a detailed analysis of its technical feasibility for fusion reactors based on HCLL blanket can be found and in [12], an analysis for a high temperature fusion reactor based on a long-term DCLL blanket is presented.

The Brayton cycle, working with an ideal gas (air or helium), requires high temperature in the thermal source in order to compensate the high consumption of the compressor. The use of CO_2 as working fluid allows Brayton cycle to overcome the high demand of compression power by entering the compression stage at a higher pressure than the critical one, so that CO_2 specific volume is not as large as if it was an ideal gas. Recuperative layouts achieve high efficiencies but the cycle low pressure is very close to the critical value, which complicates the matching of the temperature profiles. It is therefore usual to split the recuperator in two heat exchangers in order to enhance their effectiveness. Such layout is known as re-compression cycle due to the use of an auxiliary compressor. Dostal compiled the fundamentals of the cycle and deepened in its performance, including heat exchanger designs, economy and turbomachinery [13]. Sarkar et al. [14] conducted a second law analysis of a S-CO_2 power cycle, founding another one based on entropy generation in [11]. The most outstanding feature of S-CO_2 cycles with respect to Rankine ones is probably their remarkable compactness. Other characteristics, though, are less favorable. Precooling, for instance, is rather complex. If the cycle low pressure is near the critical one (typically 75 bar), CO_2 specific heat experiences a very sharp peak at low temperatures, hindering heat transfer. Additionally, such low pressures mean heat rejection at very low temperature differences, which requires high water mass flow rates (i.e., a high pumping power) at the secondary side of the heat exchanger. These issues can be overcome by increasing the suction pressure to around 85 bar, being this value a right balance between CO_2 properties variation and efficiency [11].

Three issues have been identified in the S-CO_2 Brayton cycle: compressor stability, turbomachinery design and low performance of scaled prototypes. The expected compressor stability problems are related with the sharp variation of properties near the critical point, changing from liquid to vapor typical values. Baltadjiev et al. [15] forecast stability problems due to condensation of CO_2 inside the compressor, caused by acceleration. However, experimental measurements done at Sandia National Laboratory (SNL) [16] demonstrated stable operation in the steady state and the start-up, with the suction close to the critical point, even inside the dome. They justified this stable behavior due to the low density ratio (liquid/vapor) of the CO_2 in such stages. Regarding the turbomachinery design, the main problem is found in the compressor design due to, again, its closeness to the critical point, where

the use of typical correlations for ideal gases [17] can entail to wrong solutions. Dyreby [18] overcame this issue by adjusting the non-dimensionless coefficients of turbomachinery to experimental data performed at SNL. Finally, the low performance obtained with scale prototypes is a common problem in all laboratories, due to limitations in maintaining the similarity parameters [19]. This means that performance values will be better when real-scale devices will be tested.

The expected operation of DEMO, at least in the near and mid-term, is in pulsed mode due to coil limitations [1]. This performance entails to the intermittency management of the energy source, in a similar way than in a concentrated solar plant (CSP). The technical feasibility of the S-CO_2 has also been analyzed for CSP, especially for central tower systems, where the compactness of the power plant shows integration advantages. So, SunShot Project promoted by the Department of Energy of USA seeks to develop a megawatt-scale S-CO_2 cycle optimized for the highly transient solar power plant profile [20]. In [21] a thorough description is given, including a thermal energy storage system based on molten salts to extend the operation hours. S-CO_2 power cycles show a good behavior under short solar oscillations along a day, whereas thermal energy storage systems (typically molten salts) might be used to face to longer oscillations [22]. In [23] the control strategies for CSP power plants are discussed. The former analyses entail to consider this power conversion system as an alternative to DCLL blankets in the mid-term, being included by EUROfusion in its activity program for 2014-2018 period [3].

From the experimental point of view, the first experiences were carried out by Akagawa et al. [24] working with condensation cycles (low pressure cycle below the critical point). These tests pursued the replacement of Rankine cycles for inlet turbine temperatures higher than 650 ºC. In the last years different laboratories have carried out new tests thinking of nuclear and solar applications. Sienicki et al. [25] described tests for heat exchangers at Argonne National Laboratory (ANL) and a compressor loop at Japan Atomic Energy Agency (JAEA). In the Czech Republic the stability of volumetric compressors has been investigated at Bechovice Research Institute [26], planning a future laboratory for turbomachinery analyses at Rez Nuclear Research Institute [27]. Tokyo Institute of Technology is working in an experimental compressor loop [28] and a recompression plant for power production from waste heat sources of low and intermediate temperatures [19]. Korea Atomic Energy Research Institute (KAERI) is constructing a facility for testing conversion systems at different stages: compressors, simple layout (non-recuperated) and recuperated layout (without recompression) [29]. SNL studied the Brayton power cycle using different ideal gases, far from their critical point in 2006 [30]. This analysis entailed to the S-CO_2 power cycle, constructing a compressor loop and a complete cycle in un-recuperated layout [31], a recuperated layout [32] and finally a re-compression layout [33]. Future plans include the construction of the Nuclear Energy System Laboratory/Brayton Lab, with a 10 MWe power plant for SFR in 2020 [34]. Operation has been tested by Echogen Power Systems in 2010 building a 250 kWe unit (recuperated layout but no-recompression) which was installed at American Electric

Power (Ohio) working for one year. From this experience a 7.5 MWe unit was built and tested in 2013 [35]. National Renewable Laboratory (NREL) is intending a facility to analyze the feasibility of S-CO_2 power cycle in CSP. The facility will test a unit of 10 MWe with 700 ºC of turbine inlet temperature and dry cooling conditions, collaborating with SNL and Echogen Power Systems [20]. SNL is also involved with the Indian Institute of Science (IIS) in the development of a facility with a recuperated cycle for CSP applications [36].

Special attention should be paid to the heat exchangers due to its relevant role in the cycle efficiency. The Printed Circuit Heat Exchanger (PCHE) is a rather novel heat exchanger type, formed by diffusion bonding of a stack of plates, with fluid passages photo-chemically etched on one side of each plate, by using a technique derived from that employed for electronic printed circuit boards –hence the name. Argonne National Laboratory (ANL) [37] and KAERI [38] proposed them for Generation IV designs and KAERI included them in an experimental helium loop to test a design for a fusion reactor based on an helium cooled molten lithium (HCML) blanket [39]. A benchmarking survey with actual prototypes of reactors can be found in [40], with thermal effectiveness from 92 % to 98.7 %; SNL [41] supports their use for both recuperators, heat entry to the power cycle and heat rejection from the cycle, highlighting the benefits of PCHE compactness; Mito et al. [42] draw attention to the reduced pressure drop and Gezelius [43] gave ratios of 58 to 98 MW/m^3 for PCHE against 6.2 MW/m^3 with shell and tube heat exchangers working at the same capacity and log mean temperature difference. In [44] a procedure for sizing can be found. In [45] permeation in a new design of compact heat exchanger for a fusion reactor using a DCLL blanket is analyzed, showing that when using silicon carbide as structural material the permeation is practically non-existent.

In this paper a Brayton cycle using supercritical CO_2 as working fluid is proposed as the power conversion system for a DCLL fusion reactor. The main faced issue is the integration of the available thermal sources to maximize the electricity production. Pumping consumptions in the cooling loops of the reactor and heat release from the cycle have been included in the performance assessment. Besides the electricity production, operational issues as control easiness have also been taken into account. In addition, an exergy analysis has been carried out to improve the understanding of the analyzed layouts. In short, the technical feasibility of S-CO_2 for a DEMO fusion reactor based on DCLL has been assessed.

2. METHODOLOGY

2.1. Thermal specifications of the DEMO reactor

Figure 1 shows a sketch of the balance of plant of the DEMO reactor based on the DCLL blanket. It is observed that the reactor supplies heat to the power cycle from four different thermal sources: breeding blanket cooled by lithium-lead (BBLL), breeding blanket structure cooled by helium (BBHe), divertor (DIV) and vacuum vessel (VV). Each source delivers a different amount of thermal power at different ranges of temperature, using its own cooling medium. This information is compiled in Tables 1 and 2, together with additional thermo-hydraulic data. Due to the geometry of the vessel (banana shape) in the breeding blanket cooled by lithium-lead is necessary to distinguish between the layer closer to the plasma (Inboard modules, IB) and the outer one (outboard modules, OB); it is noticeable the high pressure drop in the former due to magneto-hydrodynamic effects.

As it is sketched in Figure 1, the cooling loop between every thermal source and the power cycle has been considered. Specifications in Tables 1 and 2 entail to the thermal power absorbed by the cooling medium from the reactor. To obtain the one supplied to the power cycle it is necessary to add the pumping consumption. Pump isentropic efficiencies have been set to 85% for liquids (lithium-lead and water) and 82% for helium. Pressure drop on the coolant side of heat exchangers connecting the primary loop with the power cycle has been assumed as 1 % [46], except for the lithium-lead that a value of 10 kPa has been assumed, due to the low pressure (1 bar) at the hot stream inlet. Table 3 shows the pumping consumption at each loop together with the state points. Figure 2 shows the detailed loop in the breeding blanket cooled by lithium-lead, with two branches in parallel for IB and OB modules. In the rest of loops only one branch is necessary.

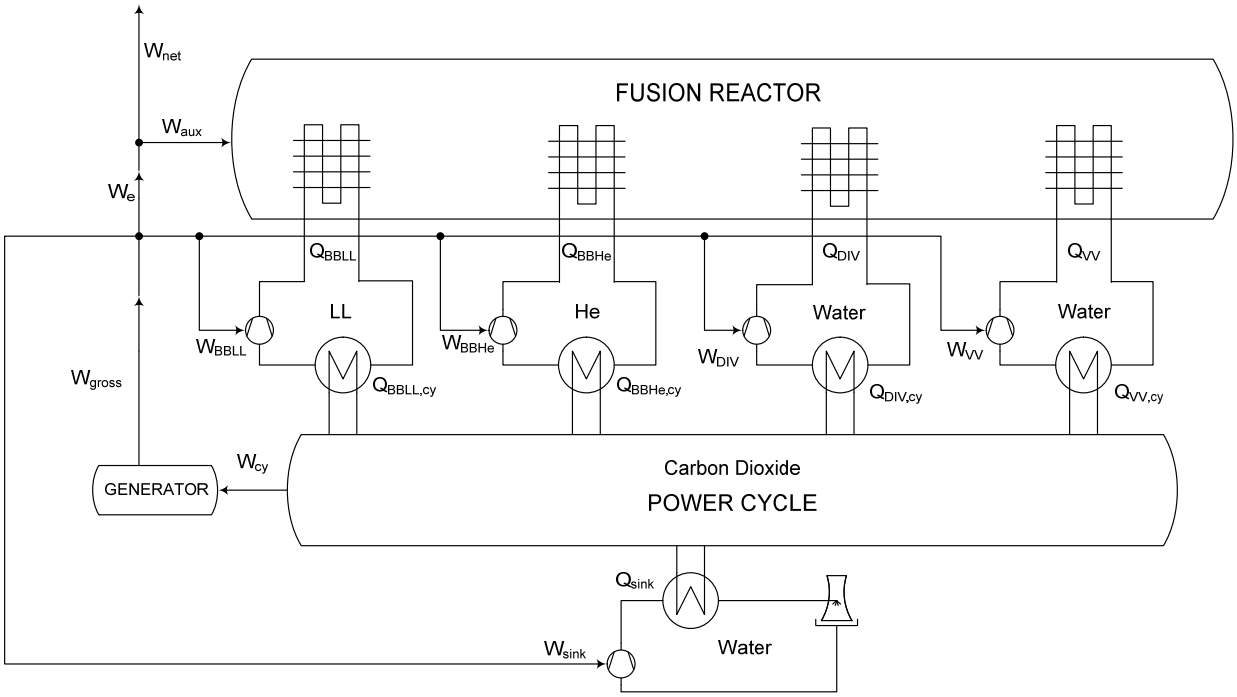

Figure 1. Energy conversion diagram in the fusion power plant.

Table 1. Specifications for Breeding Blanket [47].

		IB modules	OB modules
Coolant type	Helium	Lithium-lead	Lithium-lead
Pressure at reactor outlet [bar]	80	1	1
Temperature at reactor outlet [°C]	450	500	500
Temperature at reactor inlet [°C]	250	300	300
Pressure drop on the reactor [bar]	1.2	18	8
Density [kg/m^3]	variable	9726	9726
Mass flow rate [kg/s]	707.4	10,407.4	18,733.4

Table 2. Specifications for Divertor [48] and Vacuum Vessel [49].

	Divertor	V. Vessel
Coolant type	Water	Water
Pressure at reactor inlet [bar]	150	12
Temperature at reactor inlet [°C]	285	95
Temperature at reactor outlet [°C]	325	105
Pressure drop on the reactor [bar]	15	1
Thermal power at reactor [MW]	180	34.56

Table 3. Consumptions and state points at the cooling loops (notation according to Fig. 1. "X" denotes BBLL, BBHe, DIV or VV).

	BBLL	BBHe	DIV	VV
Heat from the reactor (Qx) [MW]	1,096	733.6	180	34.56
Heat to the cycle (Qx,cy) [MW]	1,103	757.3	182	34.67
Pumping consumption (Wx) [MW]	6.38	23.7	1.99	0.112
Reactor inlet temperature [ºC]	300	250	285	95
Reactor inlet pressure [bar]	19	81.2	150	12
Reactor outlet temperature [ºC]	500	450	325	105
Reactor outlet pressure [bar]	1	80	135	11
Pump/circulator inlet temperature [ºC]	299.8	243.7	284.4	94.99
Pump/circulator outlet pressure [bar]	0.9	79.2	133.7	10.9

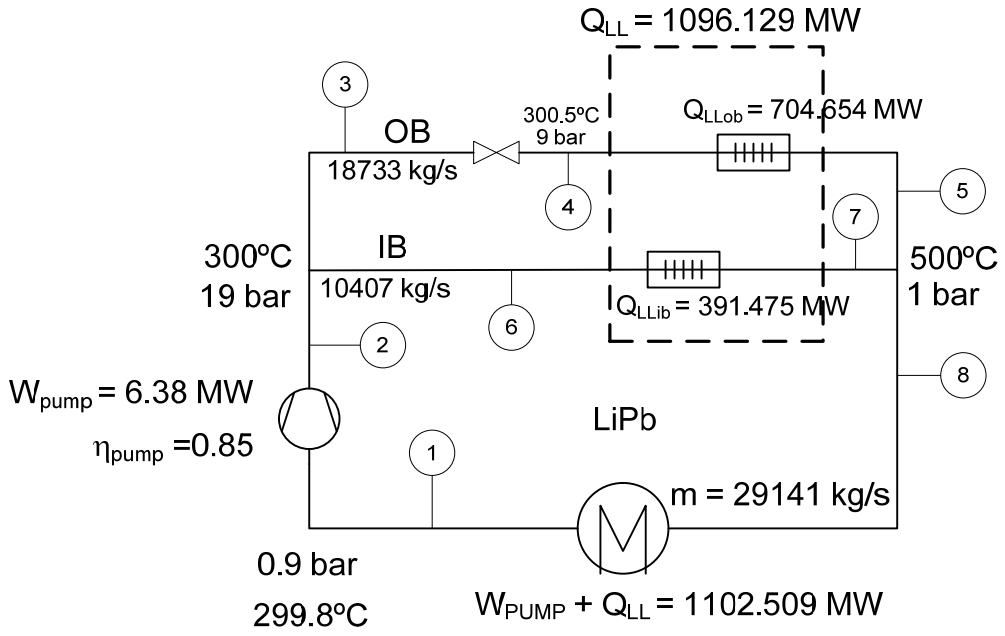

Figure 2. Primary loop in breeding blanket cooled by lithium-lead.

As in any power cycle it is necessary to release thermal power to the sink, which adds a new power consumption. This one has been obtained assuming 5 bar of overall pressure drop and 5 °C of temperature increment. These assumptions entail to assess this consumption as 2.4 % of the heat released to the sink.

Regarding to the Figure 1 it is possible to identify three different mechanical/electrical powers from the heat power released by the reactor to the busbar power:

- Cycle (W_{cy}). Net mechanical power produced by the power cycle, that is, the power produced by turbine minus the power consumed by compressors. This can be related with the heat supplied to the power cycle through the cycle efficiency (η_{cy}).
- Gross (W_{gross}). Electrical power produced by the generator. An efficiency of 97 % has been assumed [46]. This power can be related with the heat released by the reactor through the gross efficiency (η_{gross}).
- Electric (W_e). Electrical power after removing from the gross power the one required for pumping the coolants in both primary and tertiary loops (heat sink). This power can be related with the heat released by the reactor through the electric efficiency (η_e).
- Net (W_{net}). Electrical busbar power after removing from the electric power the one required for heating and current drive in the plasma and other parasitic loads. This power can be related with the heat released by the reactor through the net efficiency (η_{net}). Unfortunately overall self-consumptions (W_{aux}) have not been specified so net power cannot be assessed.

2.2 Main assumptions

In order to compare the results from the different layouts the same settings have been considered, whenever possible:

- Properties of substances. All the models have been developed in the Engineering Equation Solver (EES) environment, which includes models of pure substances [50]. So, CO_2 has been modelled as a pure substance; Helium as a pure substance except in the exergy analysis where an ideal gas model with constant specific heats has been considered; Water as a pure substance except in the exergy analysis where it has been considered as an incompressible liquid; and lithium-lead as an incompressible liquid (specific heat as 189 J/kg-K and density as 9726 kg/m^3 [51]).

- Compressor inlet. At the main compressor, conditions of 85 bar and 30 °C have been considered. This pressure exhibits a reasonable balance between the closeness to critical pressure and prevention of potential stability problems, if any [52]. Inlet auxiliary compressor conditions are 85.4 bar and temperature depending on the LTR outlet one.

- Turbine inlet. 280 bar has been taken as the turbine inlet pressure, being the temperature in a range between 380 °C to 434 °C, depending on the constrains imposed by the rest of the components in each layout (especially the pinch points at thermal sources heat exchangers).

- Heat exchangers. Printed circuit heat exchangers (PCHE) have been considered because of their excellent resistance to high pressures and their high compactness, with the possibility to achieve pinch points as small as 2 °C (effectiveness around 98 %) [40]. The approach temperature (at the heat exchanger extremes) at Low Temperature Recuperator (LTR) has been set to 7 °C in order to obtain an actual pinch point (inside the heat exchanger) close to 5 °C (always higher than 4 °C). On the other hand, the pinch point at the High Temperature Recuperator (HTR) has been set to 25 °C due to its expected small influence in the performance of the cycle [52]. In order to determine the mass flow rate through the auxiliary compressor an equal approach temperature at both extremes of the LTR has been imposed [52]. The pinch point in the rest of heat exchangers has been determined by the set of equations. The pressure drop on the CO_2 side of all the heat exchangers has been set to 40 kPa [9].

- Turbomachinery efficiency. An isentropic efficiency of 88 % has been set for compressors and 93 % for turbine, according with usual values at S-CO_2 cycles [53].

2.3 Proposed layouts

Figure 3 shows a sketch of the classical re-compression supercritical CO_2 Brayton power cycle. It is basically a recuperative Brayton cycle with two especial key points: the lower pressure in the cycle is above the critical value (around 85 bar) in order to reduce the compressor consumption due to the high density in its suction; the recuperator is split in two heat exchangers in order to enhance the matching of the temperature profiles inside the recuperator, due to the high value of the specific heat of CO_2 at low temperatures (70 ºC – 150 ºC) and high pressure, that is, in the cold stream of its low temperature section. So, the cycle integrates two recuperators, one for high temperature (HTR) and another for low temperature (LTR). In the latter, the mass flow rate of the high pressure stream is lower than the one in the low pressure stream in order to compensate the higher specific heat value of the high pressure stream. In the HTR both specific heat values are similar, so the mass flow rate is the same in both streams. In order to reduce the mass flow rate in the high pressure stream of the LTR, a fraction is bled into the auxiliary compressor (AC) before entering the precooler (PC). This fraction is mixed with the high pressure stream leaving the LTR, before entering the HTR to recover the heat from the turbine (T) outlet. The maximum efficiency is achieved when the by-passed flow rate fraction is chosen to obtain the same temperature difference at both extremes of the LTR [11]. In the precooler the cycle releases heat to the sink, being then the CO_2 suctioned by the main compressor (MC).

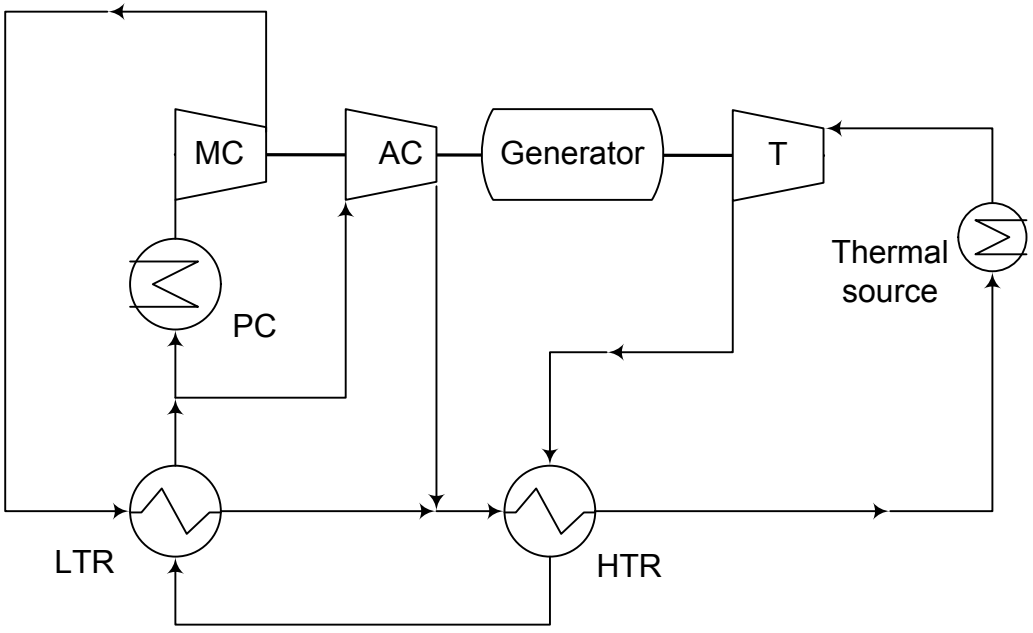

Figure 3. Classical re-compression supercritical CO_2 Brayton power cycle layout.

The classical re-compression layout has to be modified in order to integrate the different available thermal sources from the reactor. On one hand, three cases of integration have been selected: one is considering only the breeding blanket supplying heat to the power cycle (BB), other is considering both the breeding blanket and divertor (BB-DIV) and another one is including all the thermal sources (BB-DIV-VV). In each case, up to four possibilities of integration of the sources have been considered (A to D), depending of the position of each source heat exchanger. When a thermal source does not supply thermal energy to the power cycle, its heat is released to the sink. Figure 4 summarizes all the layouts analysed.

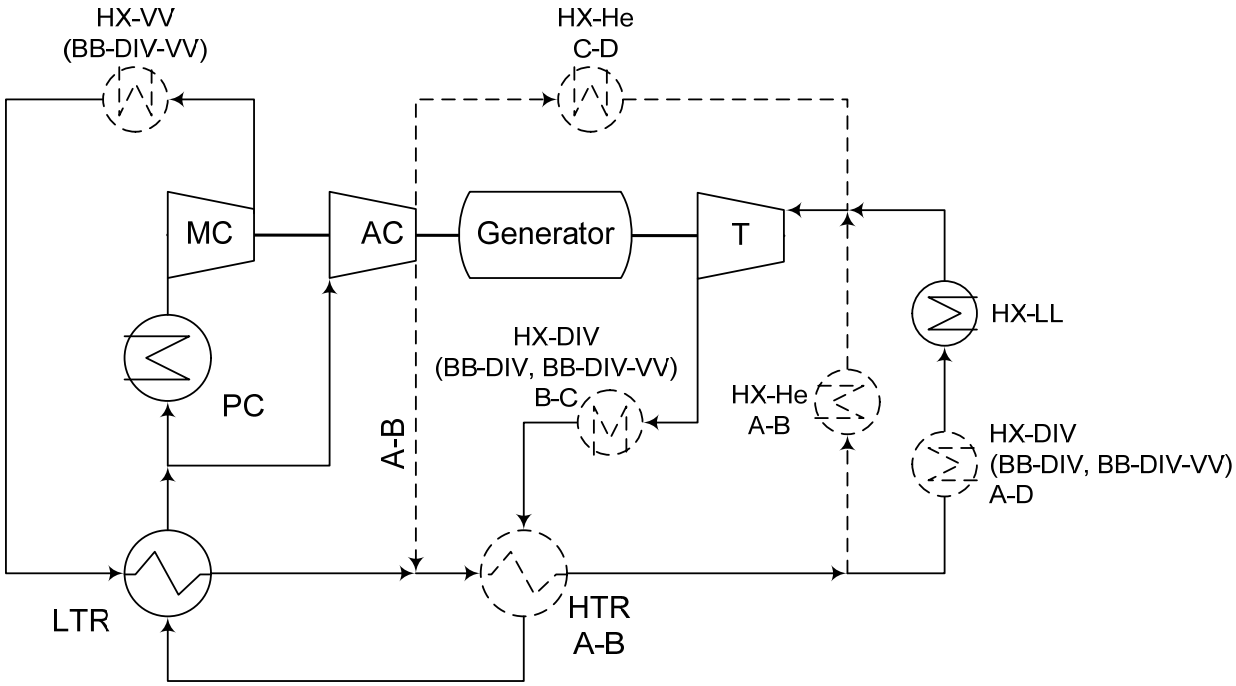

Figure 4. Summary of proposed layouts

Figure 5 gives the different layouts for the sink loop. In all the cases the water absorbs the heat released by the power cycle in the precooler. In the BB-DIV case a second loop is added to release the heat from the vacuum vessel source. Also, a third loop is added in the BB case to release the heat from the divertor source. In the second and third loops the parameters are the same than in the coolant loop for the thermal sources, where water is also employed.

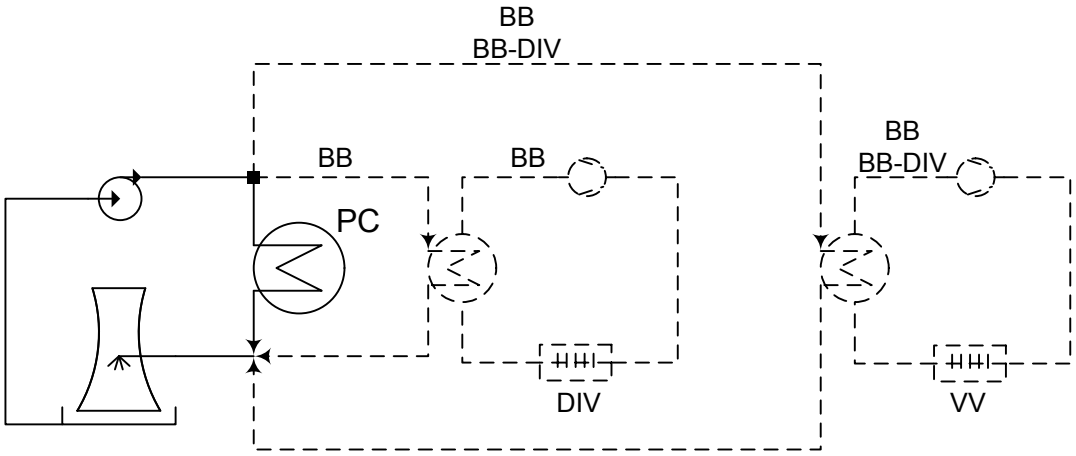

Figure 5. Summary of sink loops in each case layout

2.4. Exergy analysis

In order to interpret the changes in the performances of the layouts an exergy analysis has been carried out. The analysis has been applied to each energy loop: cooling of the reactor, power cycle and heat releasing to the sink. According to the type of fluid the entropic average temperature (Eq. 1) has been assessed in different ways.

$$T_{av} = \frac{Q_{12}}{\int_1^2 \left(\frac{\delta Q}{T} \right)} \tag{1}$$

- Average temperature of lithium-lead. The fluid is considered an incompressible liquid, so:

$$T_{LL} = \frac{C_{LL} \cdot \Delta T + \Delta p / \rho_{LL}}{C_{LL} \cdot Ln\left(\frac{T_o}{T_i} \right) + \frac{\Delta p}{\rho_{LL} \cdot \left(\frac{T_i + T_o}{2} \right)}} \tag{2}$$

- Average temperature of helium. The fluid is considered an ideal gas with constant specific heats, so:

$$T_{He} = \frac{\Delta T}{Ln\left(\frac{T_o}{T_i} \right)} \tag{3}$$

- Average temperature of water. In divertor, vacuum vessel, and sink the water is considered an incompressible liquid, so:

$$T_{W} = \frac{C_{W} \cdot \Delta T + \Delta p / \rho_{W}}{C_{W} \cdot Ln\left(\frac{T_o}{T_i} \right) + \frac{\Delta p}{\rho_{W} \cdot \left(\frac{T_i + T_o}{2} \right)}} \tag{4}$$

Equations (5) and (6) have been applied in each case:

$$C_W = \frac{\Delta u}{\Delta T} \tag{5}$$

$$\rho_W = \frac{\rho_i + \rho_o}{2} \tag{6}$$

where internal energy and density at inlet and outlet ports have been assessed considering pure substance behaviour.

- Regarding the average temperature on CO_2 side, the pressure drop (40 kPa) has been neglected, so:

$$T_{CO_2} = \frac{\Delta h}{\Delta s} \tag{7}$$

Dead state temperature (T_W^{sink}) is taken as the average temperature of water in the cooling loop (Eq. 4), with ΔT = 30-25 = 5 °C and Δp = 5 bar. Overall pressure drop on the cooling loop is included in this average temperature for simplicity. With this assumption, the average temperature is 300.5 K.

In the source loops the exergy balance is established as:

$$\left(1 - \frac{T_W^{sink}}{T_{source}}\right) \cdot Q_{source} + W_{source} = \left(1 - \frac{T_W^{sink}}{T_{cycle,c}}\right) \cdot \left(Q_{source} + W_{source}\right) + I_{PD,source} \tag{8}$$

where Q_{source} represents the heat removed from the reactor by the coolant, W_{source} the pumping work, T_{source} the average temperature of the coolant where the heat release from the reactor occurs, $T_{cycle,c}$ the average temperature of the coolant where the heat is supplied to the cycle (hot stream of the heat exchanger), and $I_{PD,source}$ is the destroyed exergy inside the heating loop due to pressure drops.

If the heat of any source (divertor and/or vacuum vessel) is released to the sink, the exergy balance is similar to the previous one (Eq.8), but $T_{cycle,c}$ represents the average temperature of the coolant where the heat is released to the cooling sink loop.

In the power cycle the exergy balance gives:

$$\sum_{sources} \left(1 - \frac{T_W^{sink}}{T_{cycle,CO2i}}\right) \cdot \left(Q_{source} + W_{source}\right) = W_{cycle} + \left(1 - \frac{T_W^{sink}}{T_{cycle,CO2o}}\right) \cdot Q_{pc} + I_{cycle} \tag{9}$$

where $T_{cycle,CO2i}$ is the average temperature of CO_2 in the heat absorption process (CO_2 side in the source heat exchangers), $T_{cycle,CO2o}$ is the average temperature of CO_2 in the heat rejection process (CO_2 side of

the pre-cooler), I_{cycle} the destroyed exergy due to internal irreversibilities in the power cycle (pressure drops, compressors, turbine, mixture process…), and Q_{pc} is the heat power released by the cycle in the pre-cooler.

The exergy balance in the electric generator is:

$$W_{cycle} = W_{gross} + I_{gen} \tag{10}$$

The exergy balance in the source heat exchangers which feed the power cycle is:

$$\left(1 - \frac{T_W^{sink}}{T_{cycle,c}}\right) \cdot \left(Q_{source} + W_{source}\right) = \left(1 - \frac{T_W^{sink}}{T_{cycle,CO2i}}\right) \cdot \left(Q_{source} + W_{source}\right) + I_{HX,source-cycle} \tag{11}$$

where $I_{HX,source-cycle}$ represents the destroyed exergy due to heat transfer process.

The exergy balance in the source heat exchangers which release heat to the sink (divertor and/or vacuum vessel) is:

$$\left(1 - \frac{T_W^{sink}}{T_{cycle,c}}\right) \cdot \left(Q_{source} + W_{source}\right) = I_{HX,source-\sin k} \tag{12}$$

where $I_{HX,source-sink}$ represents the destroyed exergy due to heat transfer process. Note that in this case the exergy of the heat removed by the water in the sink loop is zero.

The exergy balance in the pre-cooler is:

$$\left(1 - \frac{T_W^{sink}}{T_{cycle,CO2o}}\right) \cdot Q_{pc} = I_{HX,pc} \tag{13}$$

with a similar interpretation than in (Eq. 12).

In the cooling sink loop the dead state temperature is set in both heat transfer processes (heat exchanger and cooling tower). So, the exergy balance reduces to:

$$W_{sink} = I_{PD,sink} \tag{14}$$

Finally, the overall exergy destruction[1] can be determined adding all the destroyed exergies in each loop:

$$I_{TOT} = \sum I_{PD,source} + I_{PD,sink} + \sum I_{HX,source-cycle} + \sum I_{HX,source-sink} + I_{HX,pc} + I_{cycle} + I_{gen} \qquad (15)$$

Equation 15 will allow to identify the causes of improvement of one layout with respect to the others comparing the behaviour of the destroyed exergy terms.

This overall exergy destruction can be alternatively assessed as:

$$I_{TOT} = \sum_{sources} \left(1 - \frac{T_W^{sink}}{T_{source}}\right) \cdot Q_{source} - W_e \qquad (16)$$

which reveals the significance of the destroyed exergy in the reduction of the electric power generated by the balance of plant. That is, the maximum electric power achievable would be given by Eq. 17, which implies the overall exergy destruction is zero.

$$W_e^{\max} = \sum_{sources} \left(1 - \frac{T_W^{sink}}{T_{source}}\right) \cdot Q_{source} \qquad (17)$$

[1] The analysis finishes at electric power, that is, neglecting auxiliary loads due to they are unknown.

3. RESULTS

3.1 Layouts analysis

Table 4 gives the source heat exchanger pinch points. It is seen that the lithium-lead heat exchanger, with the maximum thermal power at the highest temperature, achieves its best matching (lowest pinch points) in C and D layouts, being the worst in B ones. The opposite situation occurs with the helium heat exchanger, because to match it well it is necessary to put it in parallel with the lithium-lead heat exchanger, so limiting the CO_2 inlet temperature to the lithium-lead heat exchanger. Regarding the divertor heat exchanger, its matching depends on the helium heat exchanger position. So, to locate the divertor heat exchanger upstream of lithium-lead heat exchanger or downstream the turbine produces low pinch points if the helium heat exchanger is not in parallel with the lithium-lead one (C and D layouts). Finally, high pinch points are always achieved at the vacuum vessel heat exchanger due to its low temperature forces its location, not well integrated into the power cycle.

Table 4. Source heat exchanger pinch points

		HX-LL	HX-He	HX-DIV	HX-VV
BB	A				
	B	61.3	5.2		
	C	5.5	22.8		
	D				
BB-DIV	A	34.1	5.2	45.9	
	B	61.9	5.8	30.8	
	C	9.6	55.9	4.2	
	D	5.2	62.7	9.9	
BB-DIV-VV	A	34.1	5.1	45.8	36.6
	B	61.2	5.1	30.8	36.7
	C	9.7	54.6	4.2	36.7
	D	5.2	61.3	9.9	36.7

Table 5 shows the turbine inlet temperature and turbomachines power. It is observed that the B layout always produces the low temperature. Regarding the power, although the compressor consumption is the lowest at BB case, the turbine power is also the lowest. These low values are due to the lower mass flow rate in this case because of the lower heat supplied.

Table 5. Turbomachinery performances.

		Turbine inlet temperature [ºC]	Turbine power [MW]	Main Compressor Consumption [MW]	Auxiliary Compressor Consumption [MW]
BB	A				
	B	399	1,087	177.9	184.9
	C	434	1,086	172.3	155.2
	D				
BB-DIV	A	399	1,193	195.7	203.3
	B	380	1,173	200.1	207.9
	C	410	1,170	194.4	176.6
	D	412	1,182	193.4	181.9
BB-DIV-VV	A	398	1,199	196.9	210.5
	B	380	1,179	201.1	214.9
	C	410	1,177	195.3	183.3
	D	412	1,190	194.3	189.0

Table 6 gives the generated power as well as the electric efficiency. The electric power is also depicted in Figure 6 where it is observed a relevant improvement when divertor is also supplying heat to the power cycle, although the additional inclusion of vacuum vessel is nearly negligible. In fact, the best result without divertor (B-BB) is worse than the worst one with divertor (B-BB-DIV and B-BB-DIV-VV).

Regarding layouts BB-DIV and BB-DIV-VV, option B produces between 30 and 40 MW less than other arrangements, achieving C and D the best results (differences around 1 %), followed by A (around 2 % lower than D). So, from the point of view of produced power it is recommended the scheme BB-DIV, being necessary to assess additional aspects (as control issues and behaviour at pulsed mode operation) to decide between options A, C or D. BB-DIV-VV layouts have been discarded due to the low difference in performances and to the seeking of the size minimization of the heat exchangers (in BB-DIV the vacuum vessel heat exchanger releases the heat to the sink so it works with a higher pinch point and therefore with lower size).

Table 6. Generated power (cycle, gross and electric) and electric efficiency.

		Cycle power [MW]	Gross power [MW]	Electric power [MW]	Electric efficiency [%]
BB	A				
	B	724.2	702.5	638.0	31.2
	C	758.1	735.4	671.7	32.9
	D				
BB-DIV	A	794.4	770.5	707.7	34.6
	B	764.8	741.8	678.3	33.2
	C	799.4	775.4	712.7	34.9
	D	807.0	782.8	720.3	35.2
BB-DIV-VV	A	791.7	767.9	705.0	34.5
	B	763.3	740.4	676.9	33.1
	C	798.8	774.8	712.1	34.8
	D	806.5	782.3	719.7	35.2

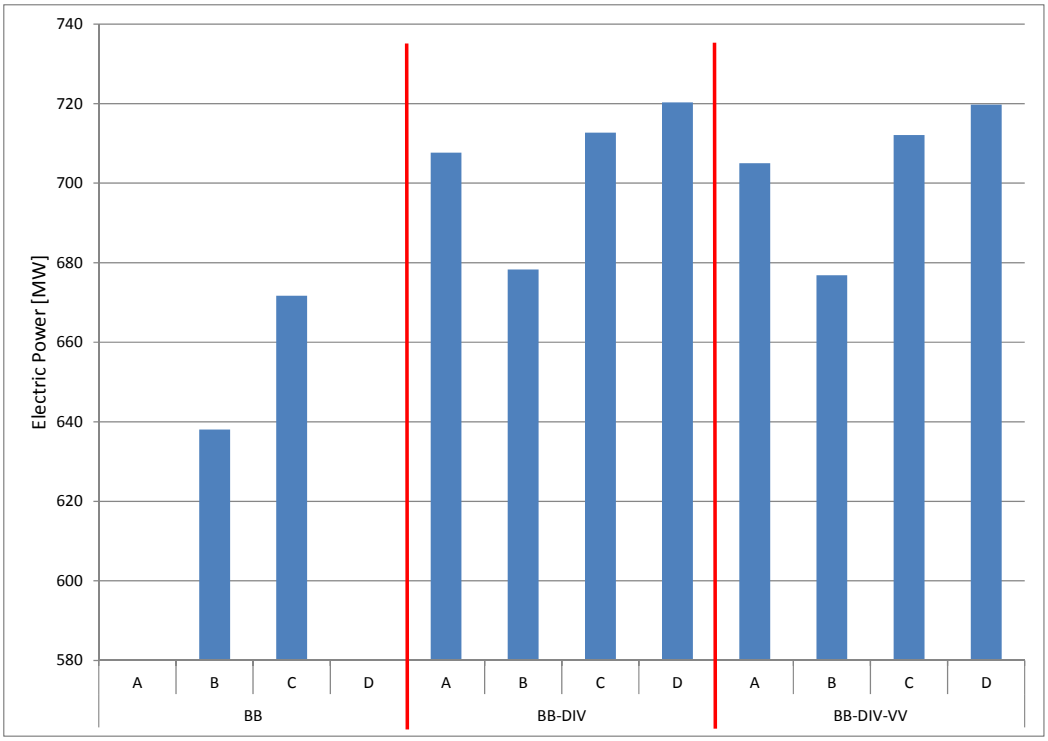

Figure 6. Electric power produced in each proposed layout.

Another selection criterion is the complexity in the associated control system. Although a dynamic study is required to assess the controllability of each layout, some ideas on the relative difficulty of controlling layouts A, C and D can be anticipated if the control objective is to achieve a pre-defined CO_2 temperature at the outlet of the three source heat exchangers. Compared with A, layouts C and D offer the possibility of controlling the flow through AC and HX-He by one single valve. The fact that HX-DIV and HX-LL are connected in series upstream of the turbine in layouts A and D makes it possible to control their flow rate by means of a single valve. In layout C, the control of the flow rate through HX-DIV will need an additional valve and this seems to interfere more with the performance of the rest of the plant than in layouts A and D. Nevertheless, the control system will have other additional objectives (e.g. it can be required to control the lithium-lead and helium temperatures at the outlet of the heat exchangers, before the fluid returns to the breeding blanket and the divertor); this fact makes too difficult to assess the relative controllability without a detailed analysis.

Finally, another criterion to select the proposed layout is the operation under pulsed mode condition. So, the work of reactor in DEMO will be intermittent, releasing heat from the plasma during 2 hours, followed by a shutdown of 0.5 hour [3]. This operation mode will require the integration of a thermal energy storage system which can replace the heat supply when plasma is shutdown. Taking into account this fact the most suitable layouts will be the A ones, in which all the thermal sources can be located in a source island connected to the power cycle between the high temperature recuperator and the turbine.

3.2. Exergy analysis

Figures 7, 8 and 9 show the results of an exergy analysis to better understand the behaviour of each layout. The low level of integration in layouts BB produces a lower destruction of exergy inside the cycle regards BB-DIV and BB-DIV-VV; however, the release of the heat from the divertor to the sink entails to a higher exergy destruction in BB cases than in the rest. Focusing on BB-DIV cases (the analysis is similar to BB-DIV-VV), layout B is characterized by a high exergy destruction in lithium-lead thermal source (around 35 MW higher than in the rest of cases); however, exergy destruction on helium source is the lowest in case B, comparable to case A, and around 20 MW less than in C and D. The former fact is due to the position of the helium source: in parallel with lithium-lead in cases A and B and downstream the auxiliary compressor in cases C and D.

So, the position of the thermal source in the power cycle determines the electric power achieved, being determinant the low temperature of the helium source. So, in case A it is necessary to limit the turbine inlet temperature to 399 °C; however, the position of divertor upstream the lithium-lead source controls the destroyed exergy on the latter. In fact, if divertor is moved downstream the turbine and the helium source is maintained at the same position (case B) the destruction of exergy on lithium-lead achieves the maximum value, being necessary to reduce the turbine inlet temperature to 380 °C. Finally, when the helium source is situated downstream the auxiliary compressor (cases C and D) the turbine inlet temperature can be increased (more than 410 °C), reducing the exergy destruction at the lithium-lead source to similar values than in case A. In addition, the destroyed exergy at the helium source is increased, but achieving values 15 MW lower than the destroyed exergy at the lead-lithium in case B.

Another noticeable issue is the lower reduction of exergy destruction inside the cycle in cases C and D regards A and B. This fact is due to the suppression of HTR in C and D layouts by the new connections downstream the auxiliary compressor.

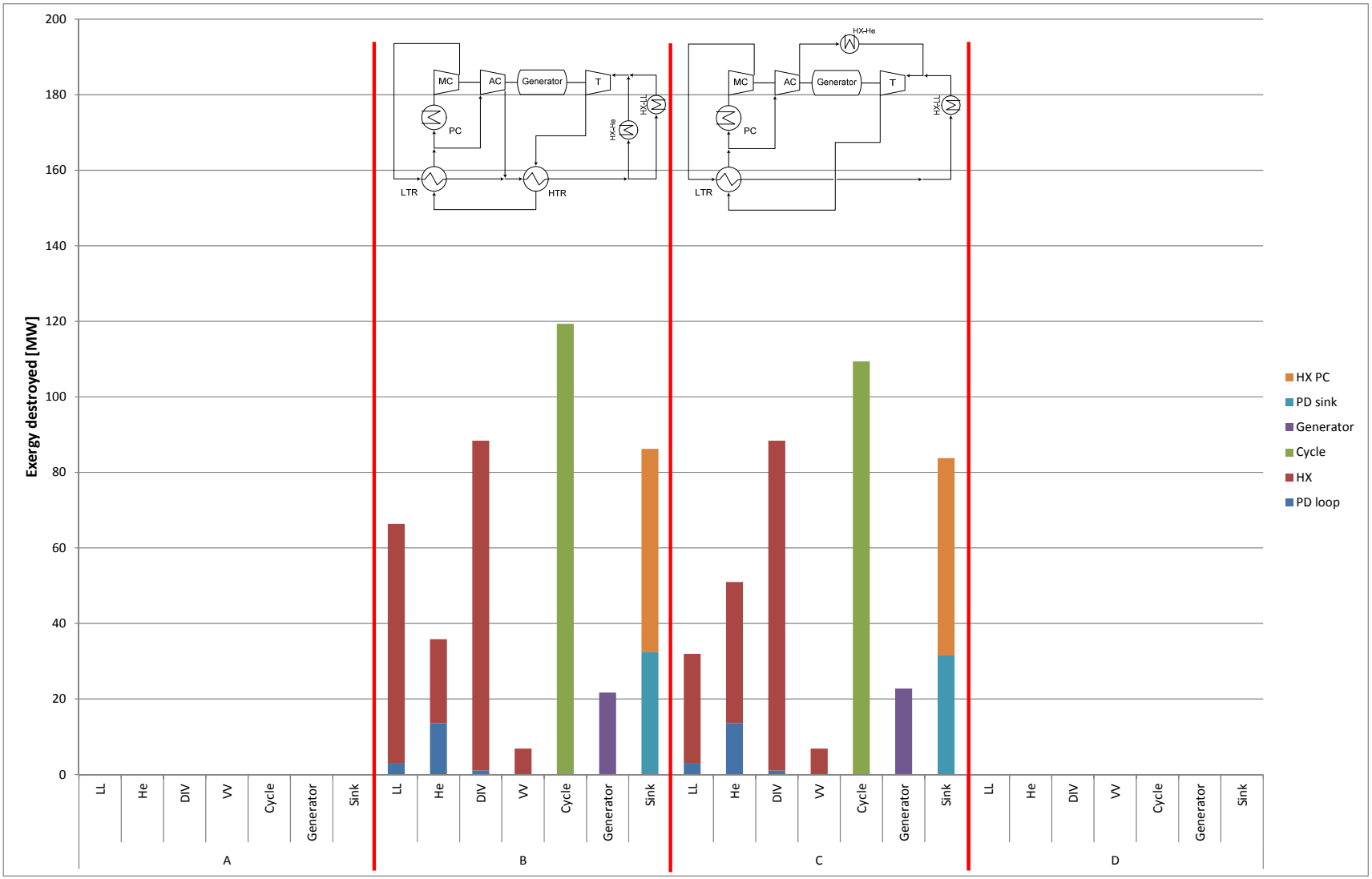

Figure 7. Exergy analysis in BB layouts.

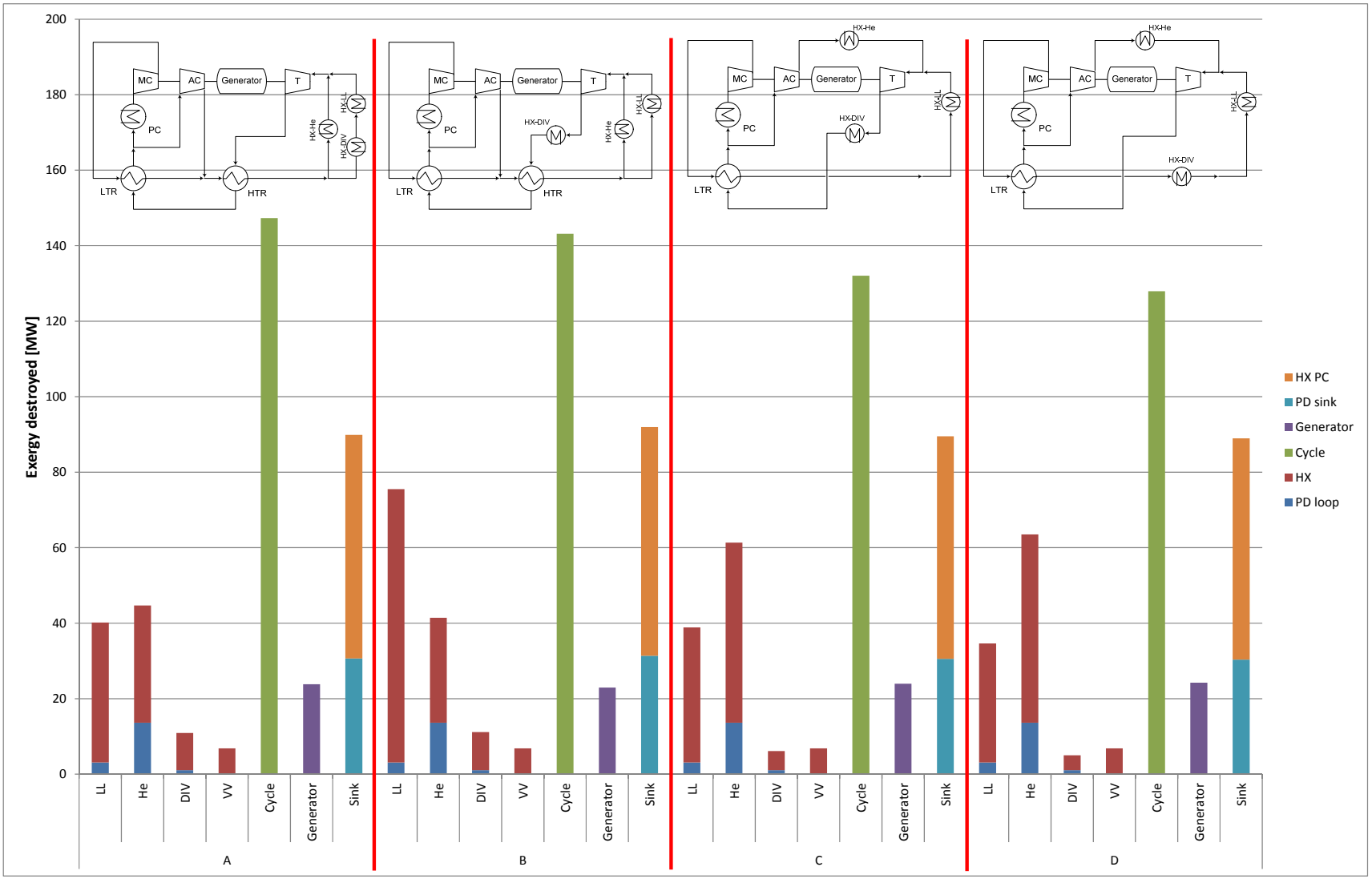

Figure 8. Exergy analysis in BB-DIV layouts

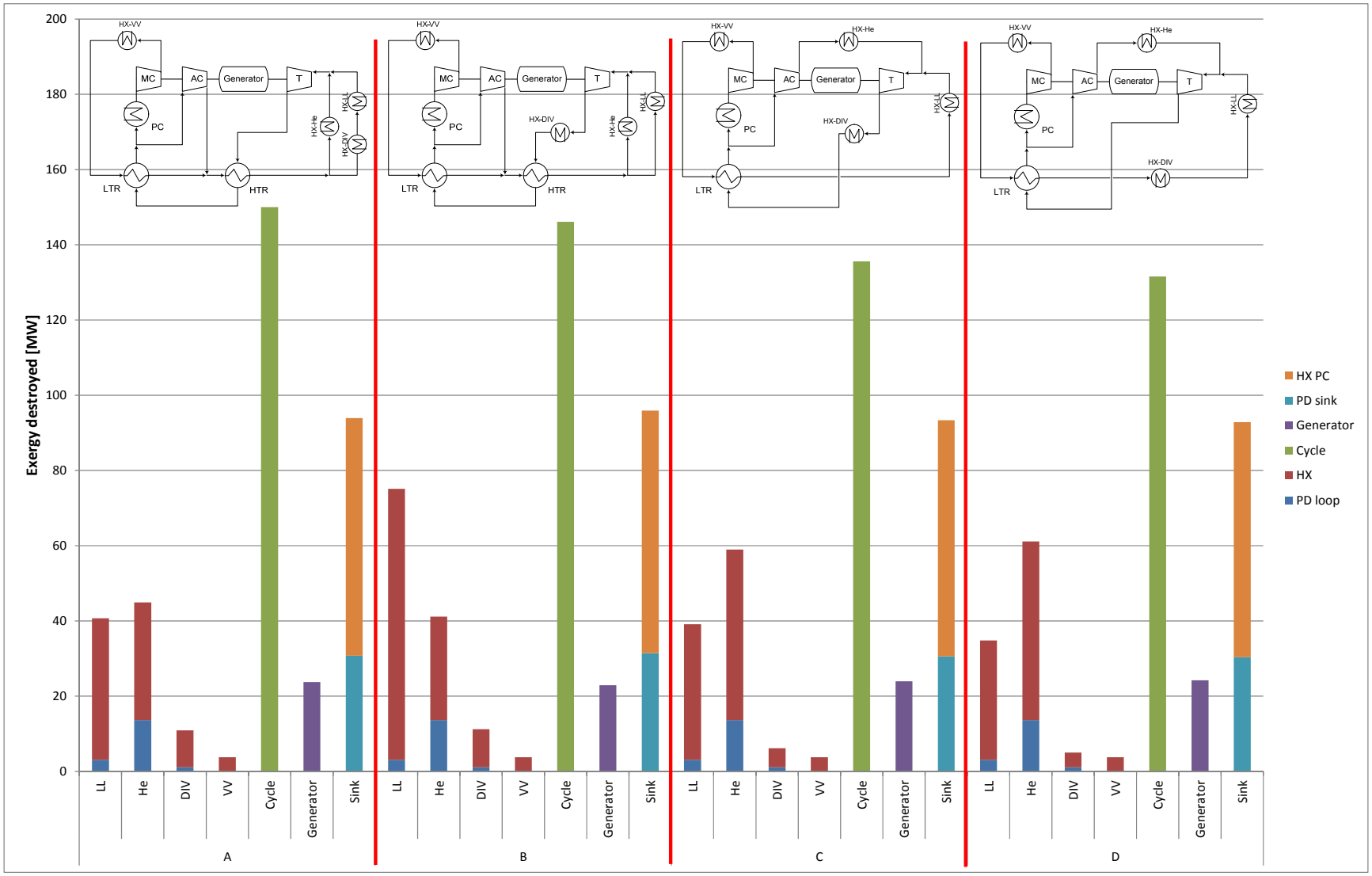

Figure 9. Exergy analysis in BB-DIV-VV layouts.

3.3 Proposed layout

Taking into account the previous considerations about control and integration of the thermal energy system, as well as the little improvement achieved when supplying the heat to the power cycle, the proposed configuration is the case BB-DIV with layout A. This option hardly losses 1.7 % of electric power with respect to the best case (layout D in case BB-DIV-VV), but integrates all the thermal sources in a single island, being easy to shift between the thermal energy system and the actual sources. Figure 9 sketches the layout, Table 7 gives the state points and Figure 10 plots the T-s diagram. The turbine mass flow rate is 9,750 kg/s, 6,879 kg/s in the main compressor, and 2,871 kg/s in the auxiliary. Regarding to the sink heat exchangers, the heat released at the precooler is 1,248 MW and the pumping consumption in the loop crossing the cooling tower is 30.7 MW. In the recovering system 2,502 MW are exchanged, belonging 85.7 % to the LTR, with a pinch point of 4.2 ºC and the rest to the HTR, with a pinch point of 25 ºC.

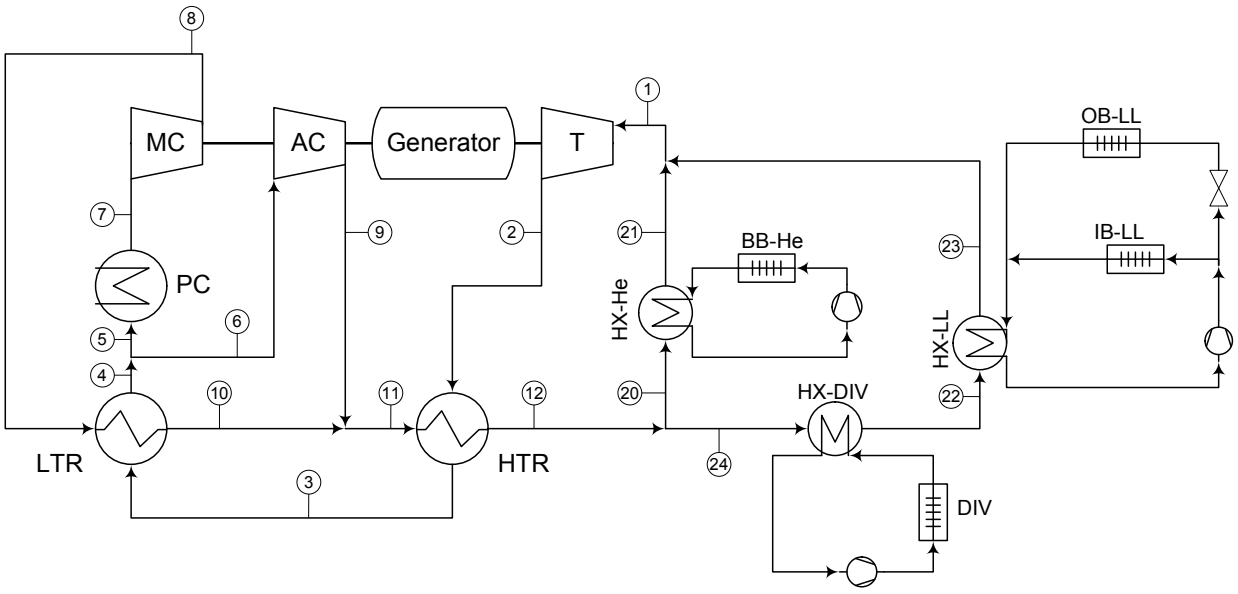

(a) Power cycle layout

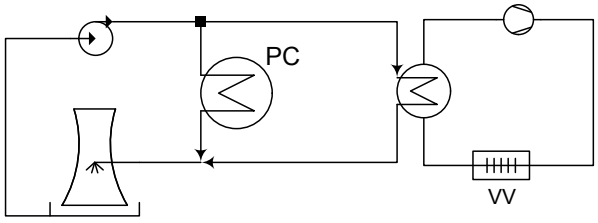

(b) Sink loop

Figure 10. Proposed configuration: (a) power cycle layout and (b) sink loop.

Table 7. State points in A-BB-DIV.

i	T [ºC]	p [bar]	h [kJ/kg]	s [kJ/kg-K]
1	399.0	280.0	333.16	-0.3255
2	270.3	86.2	210.77	-0.3085
3	237.8	85.8	173.96	-0.3774
4	65.3	85.4	-45.87	-0.9093
5	65.3	85.4	-45.87	-0.9093
6	65.3	85.4	-45.87	-0.9093
7	30.0	85.0	-227.21	-1.4842
8	58.3	281.6	-198.76	-1.4738
9	172.6	281.2	24.94	-0.8902
10	230.8	281.2	112.81	-0.7046
11	212.8	281.2	86.94	-0.7569
12	238.5	280.8	123.74	-0.6828

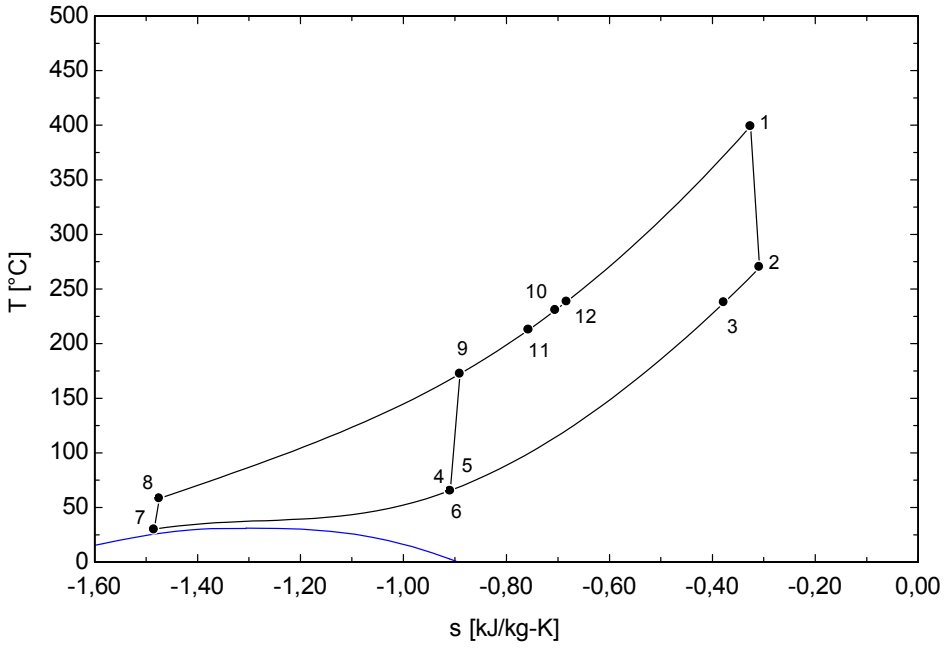

Figure 11. T-s diagram of A-BB-DIV.

4. CONCLUSIONS

This paper presents an exploratory study about alternative power conversion systems for a DEMO fusion reactor based on DCLL blanket under the framework of the EUROfusion Program 2014-2018. The power conversion system analysed has been the re-compression supercritical CO_2 Brayton power cycle. Such cycle has received clear support for advanced fission power plants, especially in Sodium Fast Reactors, and for concentrated solar power plants. This strong support has been revealed in plenty of literature and has entailed to the development of several experimental facilities along the world. Some authors have proposed this power cycle as an alternative to steam Rankine cycle for future fusion reactors.

The main analysed issue has been the integration of the four thermal sources (two from the blanket, one for the divertor and one from the vacuum vessel), with different amounts of heat and temperature range. The first step has been to define the source loop, to remove the heat from the reactor, and the sink loop to release the heat from the thermodynamic cycle, and eventually the heat released directly to the sink from some sources. Pumping consumptions in both loops have been taken into account in the assessment of the electricity production. Once the overall chain of power from the reactor to the sink has been defined, a total of 10 scenarios have been analysed, considering the supplying of heat from the reactor to the power cycle in three cases (blanket, blanket plus divertor, and blanket plus divertor plus vacuum vessel). Up to four layouts have been analysed in each case, depending on the location of the thermal sources. The assessment of each scenario has taken into account the maximization of electricity production as well as issues of control and thermal energy storage systems integration. Finally, an exergy analysis has been carried out in order to understand the behaviour of the different scenarios.

The main amount of thermal power comes from the blanket, so this source has always been included. The contribution from the divertor to the electric power generation has resulted very relevant, achieving increases up to 12.9 % in the electricity production. However, the inclusion of the vacuum vessel, with low thermal power and low temperature level, has a small effect in the improvement of the electricity generation; increasing the complexity of the layout, control system and storage integration. Regarding the location of thermal sources in the power cycle, the position of the heat exchanger taking the heat from the zone of the blanket cooled by helium has revealed as decisive, achieving the highest electricity production when it is situated downstream the auxiliary compressor in all the considered positions for the divertor. In spite of these considerations, the maximum increase between the four considered scenarios when the heat from the blanket and the divertor is supplied to the power cycle is around 6 %, being lower than 2 % if the worst scenario is neglected.

The destroyed exergy is well explained by the heat exchangers integration due to the low pressure drops considered, except in the sink loop. So, the exergy analysis carried out at source loops entails to similar

conclusions than the study of the pinch points of the source heat exchangers. So, the heat release to the sink from the divertor destroys a lot of exergy, being decisive the location of the helium cooled blanket heat exchanger. It is also observed as the simplicity in the layout (suppression of some devices) allows reducing the exergy destruction inside the thermodynamic cycle.

Results obtained clearly entail to select the BB-DIV case (heat from the vacuum vessel released directly to the sink). Among the four layouts considered, B (helium heat exchanger in parallel with the lithium-lead one and divertor heat exchanger downstream the turbine) is clearly the worst, but there is less than 2 % of variation in the electricity production among the other three layouts. Control considerations suggest D as the optimal one, with also a good behaviour in the A layout. Taking into account the integration of energy storage in order to face the pulsed mode operation the A layout prevails among the others due to all the thermal sources are joined in an island. So, as the electricity production from A layout is hardly 2 % lower than in D, the former is proposed as the energy conversion system of the DEMO reactor analysed based on DCLL blanket, achieving an electric power of 707.7 MW and an electric efficiency of 34.6%. Dynamic analysis should be performed in order to assess the actual controllability.

ACKNOWLEDGMENT

This work has been carried out within the framework of the EUROfusion Consortium and has received funding from the Euratom research and training programme 2014-2018 under grant agreement No 633053. The views and opinions expressed herein do not necessarily reflect those of the European Commission.

References

[1] F. Romanelli, “Fusion electricity: a roadmap to the realization of fusion energy”, EFDA, ISBN 978-3-00-040720-8, November 2012.

[2] L.V. Boccaccini, A. Aiello, O. Bede, F. Cismondi, L. Kosek, T. Ilkei, J.-F. Salavy, P. Sardain, L. Sedano, European TBM Consortium of Associates, Present status of the conceptual design of the EU test blanket systems, Fusion Engineering and Design 86 (2011) 478-483.

[3] E. Cipollini, Primary Heat Transfer System (PHTS) & Balance of Plant (BOP) Project. Project Management Plan (PMP). EFDA_D_2LF339 (2014).

[4] D. Maisonnier et al., A conceptual study of commercial fusion power plants. Final Report of the European Fusion Power Plant Conceptual Study (PPCS), EFDA-RP-RE-5.0, April 13th, 2005.

[5] J.I. Linares, L.E. Herranz, B.Y. Moratilla, I.P.Serrano, Power conversion systems based on Brayton cycles for fusion reactors, Fusion Engineering and Design 86 (2011) 2735-2738.

[6] L.E. Herranz, J.I. Linares, B.Y. Moratilla, Power cycle assessment of nuclear high temperature gas-cooled reactors, Applied Thermal Engineering 29 (2009) 1759–1765.

[7] G.D Pérez-Pichel, J.I. Linares, L.E. Herranz, B.Y. Moratilla, Thermal analysis of supercritical CO_2 power cycles: Assessment of their suitability to the forthcoming sodium fast reactors, Nuclear Engineering and Design 250 (2012) 23-34

[8] G.D. Pérez-Pichel, J.I. Linares, L.E. Herranz, B.Y. Moratilla, Potential application of Rankine and He-Brayton cycles to sodium fast reactors, Nuclear Engineering and Design 241 (2011) 2643-2652

[9] M. Medrano, D. Puente, E. Arenaza, B. Herrazti, A. Paule, B. Brañas, A. Orden, M. Domínguez, R. Stainsby, D. Maisonnier, P. Sardain, Power conversion cycles study for He-cooled reactor concepts for DEMO, Fusion Engineering and Design 82 (2007) 2689-2695

[10] S. Ishiyama, Y. Muto, Y. Kato, S. Nishio, T. Hayashi, Y. Nomoto, Study of steam, helium and supercritical CO_2 turbine power generations in prototype fusion power reactor, Progress in Nuclear Energy 50 (2008) 325-332.

[11] J.I. Linares, L.E. Herranz, I. Fernández, A. Cantizano, B.Y. Moratilla, Supercritical CO2 Brayton power cycles for DEMO fusion reactor based on Helium Cooled Lithium Lead blanket, Applied Thermal Engineering 76 (2015) 123-133.

[12] I.P. Serrano, J.I. Linares, A. Cantizano, B.Y. Moratilla, Enhanced arrangement for recuperators in supercritical CO2 Brayton power cycle for energy conversion in fusion reactors, Fusion Engineering and Design 89 (2014) 1909-1912

[13] V. Dostal, A Supercritical Carbon Dioxide Cycle for Next Generation Nuclear Reactors, Massachusetts Institute of Technology, USA, 2004, (PhD Thesis).

[14] J. Sarkar, Second law analysis of supercritical CO_2 recompresion Brayton cycle, Energy 34 (2009) 1172-1178.

[15] N.D. Baltadjiev, C. Lettieri, Z.S. Spakovsky, An investigation of Real Gas Effects in Supercritical CO_2 centrifugal compressors, Journal of Turbomachinery 137 (2015) 091003.1-091003-13

[16] J.S. Noall, J.J. Pasch, Achievable efficiency and stability of supercritical CO2 compression systems, in: Supercritical CO2 Power Cycle Symposium, Pittsburgh, USA, September 9-10, 2014

[17] L. Moroz, B. Frolov, M. Burlaka, O. Grulev, Turbomachinery flowpaths design and performance analysis for supercritical CO_2, in: ASME Turbo Expo 2014: Turbine Technical Conference and Exposition, Düsseldorf, Germany, June 16-20, 2014, GT2014-25385, V02BT45A004 (8 pages)

[18] J.J. Dyreby, Modeling the supercritical carbon dioxide Brayton cycle with recompression, University of Wisconsin-Madison, USA, 2014, (PhD Thesis).

[19] M. Utamura, H. Hasuike, T. Yamamoto, Demosntration test plant of closed cycle gas turbine with supercritical CO_2 as working fluid, Strojarstvo 52 (2010) 459-465

[20] C. Turchi, T. Held, J. Pasch, K. Gawlik, 10 MW supercritical-CO2 turbine project, in: SunShot Program Review, Phoenix, USA, April 23-25, 2013

[21] Z. Ma, C.S. Turchi, Advanced Supercritical Carbon Dioxide Power Cycle Configurations for Use in Concetrating Solar Power Systems, Supercritical CO_2 Power Cycle Symposium, Boulder, Colorado, USA, May 24-25, 2011 (NREL/CP-5500-50787).

[22] B.D. Iverson, T.M. Conboy, J.J. Pasch, A.M. Kruizenga, Supercritical CO_2 Brayton cycles for solar-thermal energy, Applied Energy 111 (2013) 957-970.

[23] R. Singh, S.A. Miller, A.S. Rowlands, P.A. Jacobs, Dynamic characteristics of a direct-heated supercritical carbon-dioxide Brayton cycle in solar thermal power plant, Energy 50 (2013) 194-204.

[24] K. Akagawa, T. Fujii, T. Sakaguchi, K. Kawabata, K. Ogura, T. Kuroda, T. Miyate, Y. Ito, Studies on carbon dioxide power plant, Bulletin of the JSME 23 (1980) 238-246

[25] J.J. Sienicki, A. Moisseytsev, D.H. Cho, M. Thomas, S.A. Wright, P.S. Pickard, G. Rochau, G. Rodriguez, G. Avakian, N. Alpy, D. Haubensack, L. Gicquel, N. Simon, F. Rouillard, S. Kotake, N. Kisohara, Y. Sakamoto, J.B. Kim, J.E. Cha, J.H. Eoh, International collaboration on development of the supercritical carbon dioxide Brayton cycle for sodium-cooed fast reactors under the Generation IV International Forum. Component design and balance of plant project, in: Porceedings of ICAPP '10, San Diego, USA, June 13-17, 2010, paper 10048

[26] B. Monge, Design of supercritical carbon dioxide centrifugal compressors, University of Seville, Spain, 2014, (PhD Thesis).

[27] L. Vesely, V. Dostal, Design of experimental loop with supercritical carbon dioxide, in: Proceedings of the 22nd International Conference on Nuclear Engineering ICONE22, Prague, Czech Republic, July 7-11, 2014

[28] M. Aritomi, T. Ishizuka, Y. Muto, N. Tsuzuki, Performance test results of the supercritical CO2 compressor for a new gas turbine generation system, in: Proceedings of the 18th International Conference on Nuclear Engineering ICONE18, Xi'an, China, May 17-21, 2010

[29] Y. Ahn, J. Lee, S.G. Kim, J.I. Lee, J.E. Cha, Design consideration of supercritical CO2 power cycle integral experiment loop, Energy 86 (2015) 115-127

[30] S.A. Wright, M.E. Vernon, P. Pickard, Small scale closed Brayton cycle. Dynamic response experiment results, 2006. Sandia National Laboratory SAND2006-3485, USA.

[31] S.A. Wright, R.F. Radel, M.E. Vernon, G.E. Rochau, P.S. Pckard, Operation ans analysis of a supercritical CO2 Brayton cycle, 2010. Sandia National Laboratory SAND2010-0171, USA.

[32] T. Conboy, S. Wright, J. Pasch, D. Fleming, G. Rochau, Performance characteristics of operating supercritical CO_2 Brayton cycle, Journal of Engineering for Gas Turbine and Power 134 (2012) 111703.1-111703.12

[33] T. Conboy, J. Pasch, D. Fleming, Control of a supercritical CO_2 recompression Brayton cycle demonstration loop, Journal of Engineering for Gas Turbine and Power 135 (2013) 111701.1-111701.12

[34] D. Fleming, T. Holschuh, T. Conboy, G. Rochau, R. Fuller, Scaling considerations for a multi-megawatt class supercritical CO_2 Brayton cycle and path forward for commercialization, in: Proceedings of ASME Turbo Expo 2012 GT2012, Copenhagen, Denmark, June 11-15, 2012, GT2012-68484

[35] T.J. Held, Initial test results of a megawatt-class supercritical CO_2 heat engine, in: The 4th International Symposium – Supercritical CO2 Power Cycles, Pittsburgh, USA, September 9-10, 2014

[36] P. Garg, P. Kumar, P. Dutta, T. Conboy, C. Ho, Design of an experimental test facility for supercritical CO2 Brayton cycle, in: Proceedings of the ASME 2014 8th International Conference on Energy Sustainability ES2014, Boston, USA, June 20-July 2, 2014

[37] H. Song, Investigations of a printed circuit heat exchanger for supercritical CO_2 and water, Kansas State University, USA, 2007, (MSc Dissertation).

[38] J.E. Cha, T.H. Lee, J.H. Eoh, S.H. Seong, S.O. Kim, D.E. Kim, M.H. Kim, T.W. Kim, K.Y. Suh, Development of Supercritical CO_2 Brayton Energy Conversion System Coupled with a Sodium Cooled Fast Reactor, Nuclear Engineering and Technology 41 (2009) 1025-1044.

[39] S.B. Yum, E.H. Lee, D.W. Lee, G.Ch. Park, Model validation of GAMMA code with heat transfer experiment for KO TBM in ITER, Fusion Engineering and Design 88 (2013) 716-720.

[40] B. Halimi, K.Y. Suh, Computational analysis of supercritical CO_2 Brayton cycle power conversion system for fusion reactor, Energy Conversion and management 63 (2012) 38-43.

[41] S.A. Wright, R.F. Radel, R. Fuller, Engineering performance of supercritical CO_2 Brayton cycles, ICAPP 10, San Diego, USA, June 13-17, 2010 (paper 10264).

[42] M. Mito, N. Yoshioka, Y. Ohkubo, N. Tsuzuki, Y. Kato, Fast reactor with indirect cycle system of supercritical CO_2 gas turbine plant, ICAPP 06, Reno, Nevada, USA, June 4-8, 2006 (paper 6265).

[43] K. Gezelius, Designs of compact intermediate heat exchangers for gas cooled fast reactors, Massachusetts Institute of Technology, USA, 2004, (MSc Dissertation).

[44] I.P. Serrano, A. Cantizano, J.I. Linares, B.Y. Moratilla, Modeling and sizing of the heat exchangers of a new supercritical CO2 Brayton power cycle for energy conversion for fusion reactors, Fusion Engineering and Design 89 (2014) 1905-1908

[45] I. Fernández, L. Sedano, Design analysis of a lead–lithium/supercritical CO_2 Printed Circuit Heat Exchanger for primary power recovery, Fusion Engineering and Design 88 (2013) 2427-2430.

[46] H. Latham,P. Clarkson, Fusion Balance of Plant Assessment (under EFDA Work Package WP12-DAS08-BoP), (2LLNBX).

[47] Preliminary Input from BB (EFDA_D_2LFUG_v1.0)

[48] Preliminary Input from DIV (EFDA D 2LNTV5 v1.0)

[49] Technical specifications WP13-DAS08: Primary Het Transfer & Balance of Plant Systems, Harman, EFDA WP13-DAS08-BOP V2.3 - 24/06/2013

[50] Engineering Equation Solver: www.f-chart.com

[51] E. Mas de les Valls, L.A. Sedano, LL. Batet, I. Ricapito, A. Aiello, O. Gastaldi, et al., Lead–lithium eutectic material database for nuclear fusion technology, Journal of Nuclear Materials 376 (2008) 353–357

[52] J.I. Linares, L.E. Herranz, I. Fernández-Berceruelo, B.Y. Moratilla, A. Cantizano, Design, modelling and analysis of primary heat transfer and BoP options for integration with a DEMO fusion power plant: FINAL REPORT on supercritical CO_2 Brayton power cycles (under EFDA WP13-DAS08-T02-BOP), (2L58SM).

[53] J.S. Bahamonde-Noriega, Design method for S-CO2 gas turbine power plants, Delft University of Technology, The Netherlands, 2012, (MSc Dissertation)

Acronyms

AC	Auxiliary compressor
ANL	Argonne National Laboratory
BB	Breeding blanket
BBHe	Breeding blanket cooled by helium
BBLL	Breeding blanket cooled by lithium-lead
BoP	Balance of plant
CSP	Concentrated solar power
DCLL	Dual coolant lithium-lead
DEMO	Demonstration power plant
DIV	Divertor
EES	Engineering Equation Solver
EFDA	European Fusion Development Agreement
HCLL	Helium cooled lithium-lead
HCML	Helium cooled molten lithium
He	Helium
HTR	High temperature recuperator
HX	Heat exchanger
HX-DIV	Heat exchanger Water/CO_2 in the divertor cooling loop
HX-He	Heat exchanger He/CO_2 in the helium-cooled breeding blanket cooling loop
HX-LL	Heat exchanger lithium-lead/CO_2 in the lithium-lead-cooled breeding blanket cooling loop
HX-PC	Destroyed exergy in the precooler (in plots)
HX-VV	Heat exchanger Water/CO_2 in the vacuum vessel cooling loop
IB	Inboard
IIS	Indian Institute of Science
ITER	International Tokamak Experimental Reactor
JAEA	Japan Atomic Energy Agency
KAERI	Korea Atomic Energy Research Institute
LL	Lithium-lead
LTR	Low temperature recuperator
MC	Main compressor
NREL	National Renewable Energy Laboratory
OB	Outboard
PC	Precooler
PCHE	Printed Circuit Heat Exchanger

PD	Pressure drop
SCLL	Self-cooled lithium lead
S-CO2	Supercritical CO_2 Brayton power cycle
SFR	Sodium Fast Reactor
SNL	Sandia National Laboratory
T	Turbine
VHTR	Very High Temperature Reactor
VV	Vacuum Vessel
WCLL	Water cooled lithium lead

Notation

Latin letters

C	Specific heat
h	Enthalpy
p	pressure
Q	Heat transfer rate
s	Entropy
T	Temperature
u	Internal energy

Greek letters

δ	Infinitesimal increment
Δ	Finite increment
ρ	Density

Subscripts

av	Average
CO_2	Carbon dioxide
cy; cycle	Cycle. Referred to the net power of the cycle
cycle, CO2i	Part of the power cycle where the heat is absorbed from the thermal sources
cycle, CO2o	Part of the power cycle where the heat is rejected to the heat sink
cycle,c	Part of the cooling loop where the heat is fed to the power cycle
e	Electric
gen	Generator
gross	Gross. Referred to the electric power produced by the generator

He	Helium
HX, source-cycle	Heat exchanger which connects the thermal sources with the power cycle
HX, source-sink	Heat exchanger which connects the power cycle with the thermal sink
HX,pc	Precooler
i	Inlet
I	Destroyed exergy
LL	Lithium-lead
o	Outlet
PC	Precooler
PD	Pressure drop
PD,sink	Associated to pressure drop in the sink loop (referred to destroyed exergy)
PD,source	Associated to pressure drop in the source loop (referred to destroyed exergy)
Source	Heat source
TOT	Total
W	Water; Mechanical or Electric Power

Superscripts

Sink	Heat sink